Investigate the Performance of Prussian White $K_2Fe[Fe(CN)_6]$ Cathode for Potassium-Ion Battery

Van Hoang Luan[1,2*], Do Ngoc Nhu Quynh[1,2], Minh-Vien Le[1,2], Ly Dat[1,2], and Nguyen Tan Dat[1,2]

[1]*Faculty of Chemical Engineering, Ho Chi Minh City University of Technology (HCMUT), 268 Ly Thuong Kiet Street, District 10, Ho Chi Minh City 700000, Vietnam*

[2]*Vietnam National University Ho Chi Minh City, Linh Trung Ward, Thu Duc City, Ho Chi Minh City 700000, Vietnam*

* ***Corresponding author:***

tel: +84-702652871
email: vhluan@hcmut.edu.vn

Received: August 21, 2024
Accepted: February 9, 2025

DOI: 10.22146/ijc.99310

Abstract: *In this report, potassium iron(II) hexacyanoferrate (KFHCF) was synthesized via a precipitation method under a nitrogen-controlled atmosphere, followed by a comprehensive evaluation of its electrochemical properties. Various characterization techniques, including X-ray diffraction (XRD), scanning electron microscopy (SEM), Fourier-transform infrared spectroscopy (FTIR), and thermogravimetric analysis (TGA) are employed to investigate the structural and morphological properties of the materials. The electrochemical performance of the KFHCF materials was systematically evaluated through galvanostatic discharge cycling and cyclic voltammetry (CV) measurements. The results reveal that KFHCF material synthesized with a 2:1 molar ratio between EDTA and free Fe^{2+} ions, dried under vacuum at 100 °C for 10 h, exhibits significantly enhanced electrochemical properties compared to those with a 1:1 molar ratio. The performance was further assessed using different electrolytes, specifically K_2SO_4 and KCl. The KFHCF-based electrode demonstrates a peak current density of nearly 4 mA cm^{-2} for the redox processes of both Fe(II) coordination sites in K_2SO_4 or KCl aqueous electrolyte at a scan rate of 10 mV s^{-1}. Additionally, it delivers discharge capacities of 113.97 mAh g^{-1} (K_2SO_4) and 93.45 mAh g^{-1} (KCl) at current densities of 500 mA g^{-1}. These findings underscore the promising potential of KFHCF as an efficient electrode material for electrochemical applications.*

Keywords: *battery; electrochemistry; KFHCF; PIBs; potassium iron(II) hexacyanoferrate*

■ INTRODUCTION

Over the past decade, the growing concern about increasing energy consumption, coupled with sharp rises in the price of refined fossil fuels and the environmental impacts of their use, has made energy storage technology increasingly crucial in pursuing a sustainable society. Alternative energy sources from natural resources, such as sunlight, wind, rain, tides, and sea waves, are gaining favor as renewable energy options. However, these sources are inherently intermittent and dependent on the weather conditions. Therefore, a large-scale energy storage system that stores the generated energy is essential to balance the supply and demand of electric power and improve energy efficiency [1].

Energy storage systems can be categorized into mechanical, electrical, chemical, and electrochemical forms, depending on the types of energy within the system [2]. Rechargeable batteries, a prevalent form of electrochemical energy storage, are among the most attractive options due to their superior energy efficiency and portability, surpassing other storage methods [3]. These batteries have been developed and successfully commercialized for various electronic devices, such as lead-acid, Ni–Cd, Ni-metal hydride (NiMH), Na–S, and LIBs batteries. Since their first introduction in 1991, LiBs have dominated the portable electronics market, such as mobile phones and laptop computers, and have become integral to the advancement of electric vehicles, hybrid, and plug-in-hybrid vehicles [4].

Lithium's status as the lightest metallic element, combined with its redox potential ($E°_{Li+/Li} = -3.04$ V versus SHE), enables lithium-ion cells to operate at high voltage, offering high energy density, long cycle life, and excellent rate capability [5-8]. The small ionic radius of Li^+ facilitates its diffusion in materials, which significantly contributes to the overall efficiency of LIBs. Consequently, the demand for LIBs is rapidly increasing, as they are regarded as the major power source for portable electronic devices and next-generation vehicles. However, the key elements required for LIBs, such as Li and Co, are expensive and relatively scarce in the Earth's crust. These elements are often located in regions with uneven distribution or political sensitivity, exacerbating concerns about the long-term availability and escalating cost of these materials [9].

Despite widespread battery recycling efforts, it is unlikely that recycling alone can prevent the depletion of these resources in a timely manner. These economic and geological challenges have accelerated the search for new, low-cost, and scalable alternatives to LIBs. Potassium-ion batteries (PIBs) have emerged as a promising alternative to LIBs, offering a competitive edge over sodium-ion batteries (SIBs), due to the abundance and lower cost of potassium [10-12].

PIBs are particularly attractive due to the low standard redox potential of K^+/K ($E° = -2.93$ V versus SHE), which is only 0.11 V above that of Li. This allows rechargeable PIBs to maintain larger cell voltages [13], making them capable of higher voltage operation and relatively higher energy density than SIBs and potentially even LIBs [14]. Additionally, the lower Lewis acidity of K^+ leads to fewer solvated ions, a smaller Stokes radius, and better ionic conductivity compared to Li^+ or Na^+, which facilitates faster ion diffusion kinetics.

Another significant advantage of PIBs is the compatibility of graphite, a widely used anode material in LIBs, with reversible K^+ intercalation and deintercalation, offering a theoretical capacity of 372 mAh g^{-1}. This characteristic is less favorable for Na^+ storage [15]. Moreover, the intercalation chemistry of Li and K in positive electrode materials is quite similar, allowing the use of comparable compounds in both systems. These unique advantages position PIBs as a promising candidate for next-generation rechargeable batteries, particularly for large-scale energy storage systems and conversion applications where low cost and high-power density are critical. However, it is important to recognize that LIBs generally maintain a higher energy density than electrochemical K-ion cells. This is due to the higher equivalent weight of K compared to Li and the larger ionic radius, which decreases from 1.38 to 0.76 Å for the same series [16]. As a result, K-based cells face challenges in competing with Li-based cells regarding energy density. The unique properties of potassium continue to drive growing interest and research in PIBs technology.

Nowadays, considerable publications about cathode material have focused on studies of potassium-positive electrode materials, which can be categorized into several material groups: layered transition metal oxides, Prussian Blue analogues (PBAs), polyanionic compounds, and organic materials. Among these, PBAs stand out due to their high capacities and operational potentials, attributed to their three-dimensional (3D) open frameworks with channels and interstitial sites that facilitate the diffusion and insertion of larger K^+ ions [17]. The simplicity of synthesis, the abundance of the elements, and the unique characteristics make $K_2Fe[Fe(CN)_6]$ an attractive material for commercial applications. On top of that, the robust 3D framework structure with open channels of this compound, resulting in an exceptional variety of physical and chemical properties, has fostered intense research towards the development of electrode material for electrochemical energy storage.

Su et al. [18] synthesized $K_2Fe[Fe(CN)_6]·2H_2O$ (KFHCF) nanocubes using ethylene glycol as a solvent by a low-temperature solvothermal method and examined its electrochemical characteristics in aqueous PIB. Galvanostatic charge-discharge tests were performed under different current densities in the voltage range from 0 to 1.2 V when the CV test was carried out at various scan rates (from 0.2 to 50 mV s^{-1}), and the discharge capacity of 120 mAh g^{-1}. In this research, the KFHCF was synthesized by the

precipitation method with the aid of ethylenediaminetetraacetic acid (EDTA) as a chelating agent and an additional source of potassium ions. Controlling the size and morphology of KFHCF through reaction kinetics and the amount of EDTA plays a crucial role in enhancing the efficiency and effectiveness of the precipitation process, making it a valuable technique for producing high-quality materials for both industrial and research purposes. The electrochemical performance of the cathode material was compared using two different electrolytes (KCl and K_2SO_4). The shift of redox peak in CV and CD results demonstrated the influence of the different electrolytes. Besides, the capacity of KFHCF material obtained 113 mAh g^{-1} under K_2SO_4 electrolyte.

■ EXPERIMENTAL SECTION

Materials

Ethylenediaminetetraacetic acid dipotassium salt tetrahydrate (EDTA-2K·$4H_2O$, 99.95%) was purchased from Kermel. $FeCl_2$·$4H_2O$ (99.95%), $K_4Fe(CN)_6$·$3H_2O$ (99.5%), $(NH_4)_6Mo_7O_{24}$·$4H_2O$ (99.5%), and K_2SO_4 (99%) were all provided by Xilong. Ethanol (C_2H_5OH, 99.95%) was supplied by Comeco. Vulcan Carbon XC-72R was purchased from Cabot Corp. Nafion (5% in a mixture of aliphatic alcohols and water, $C_7HF_{13}O_5S$-C_2F_4) was purchased from Sigma. Nitrogen gas (N_2) (99.99%) and distilled water were used throughout the reaction.

Instrumentation

The morphology of prepared samples was analyzed using a scanning electron microscope (SEM, Hitachi S-4800). The as-prepared sample's crystal phase can be determined from XRD patterns, allowing Cu-Kα (λ = 0.154184 nm) radiation from an X-ray source of a Brucker (German AXS, D2 phaser A26-X1-A2B0B0B). Thermogravimetric analysis (TGA, PT1600, Germany) was employed to monitor the weight changes of the sample over time under controlled temperature variations. Fourier-transform infrared spectroscopy (FTIR, Invenio S, Bruker) was applied to investigate the vibrational modes of molecules. CV and discharge tests were carried out to evaluate the electrochemical characteristics of KFHCF material by a Model VSP-3e Bio-Logic (Science Instrument, France). All experiments were conducted using Screen Printed Electrodes (Zensor, Taiwan).

Procedure

Synthesis of Prussian white $K_2Fe[Fe(CN)_6]$

Firstly, 100 mL of distilled water was purged in nitrogen gas for 20 min before use. EDTA-2K·$4H_2O$ (2 or 4 mol) and $FeCl_2$·$4H_2O$ (2 mol) were then dissolved in 50 mL of nitrogen-purged distilled water to prepare solution A, containing $Fe[EDTA]^{2-}$ complex. Simultaneously, solution B was prepared by dissolving $K_4Fe(CN)_6$·$3H_2O$ (2 mol) in another 50 mL of distilled water, also purged with nitrogen gas. Subsequently, solution A was added dropwise to solution B over 10 min, with continuous magnetic stirring under N_2 protection. The solution was left aged for 4 h without stirring. The resulting precipitates were collected by washing, followed by centrifugation at 6000 rpm. The washing and centrifugation steps were repeated four times using distilled water and ethanol. Finally, the precipitates were then dried under vacuum at 80,100, 120, or 140 °C for 10 h as shown in Scheme 1.

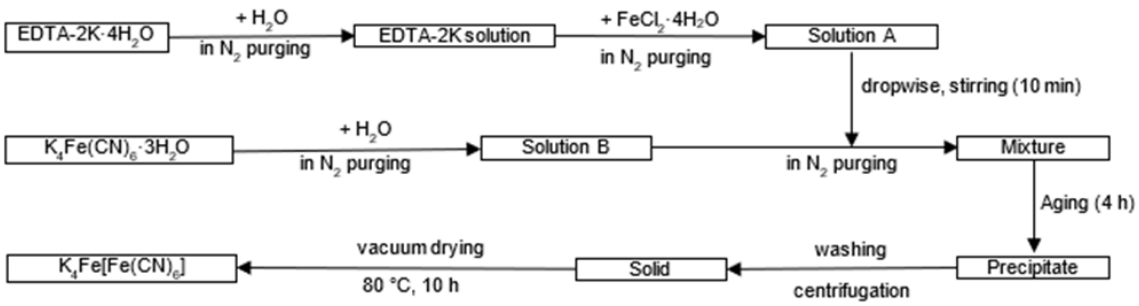

Scheme 1. Diagram of Prussian white KFHCF preparation

Electrochemical characterizations

The mixture of KFHCF (8 mg) and Vulcan Carbon XC-72R (1 mg) with a mass ratio of 8:1 was dispersed in 1 mL distilled water and 0.1 mL Nafion solution by ultrasonic for 3 min. Then, 5 µL of the mixture was loaded onto the surface of the carbon electrode and let dry at ambient temperature for 5 min or until completely dried. All the experiments were conducted at room temperature, using a three-electrodes system, including a carbon working electrode and counter electrode, Ag/AgCl reference electrode (Screen Printed Electrodes, Zensor, Taiwan) in an aqueous electrolyte. The electrodes were immersed in a saturated aqueous electrolyte (K_2SO_4 or KCl).

The CV and galvanic charge-discharge tests were performed to evaluate the electrochemical characterizations of KFHCF material during electro-oxidation reactions. The discharge capacity was measured using a Model VSP-3e Bio-Logic (Science Instrument, France). The voltage range was set between 0.0 and 1.2 V, with a scan rate of 10 mV s^{-1} for the CV test.

■ RESULTS AND DISCUSSION

The crystal structures of the KFHCF samples synthesized with 1:1 and 2:1 molar ratios of a chelating agent (EDTA) to Fe^{2+} at different drying temperatures (80, 100, 120, and 140 °C) were characterized using XRD patterns, as shown in Fig. 1(a). From the XRD results, it was demonstrated that all the samples obtained from the above synthesis method exhibited typical Prussian white patterns (JCPDS No. 31-1000) with diffraction angles at 2θ = 17.58, 24.92, 30.92, 35.60, 40.04, 44.14, 51.29, respectively. These angles correspond to the (200), (220), (222), (400), (420), (422), and (440) planes, respectively. The diffraction peaks can be attributed to a face-centered

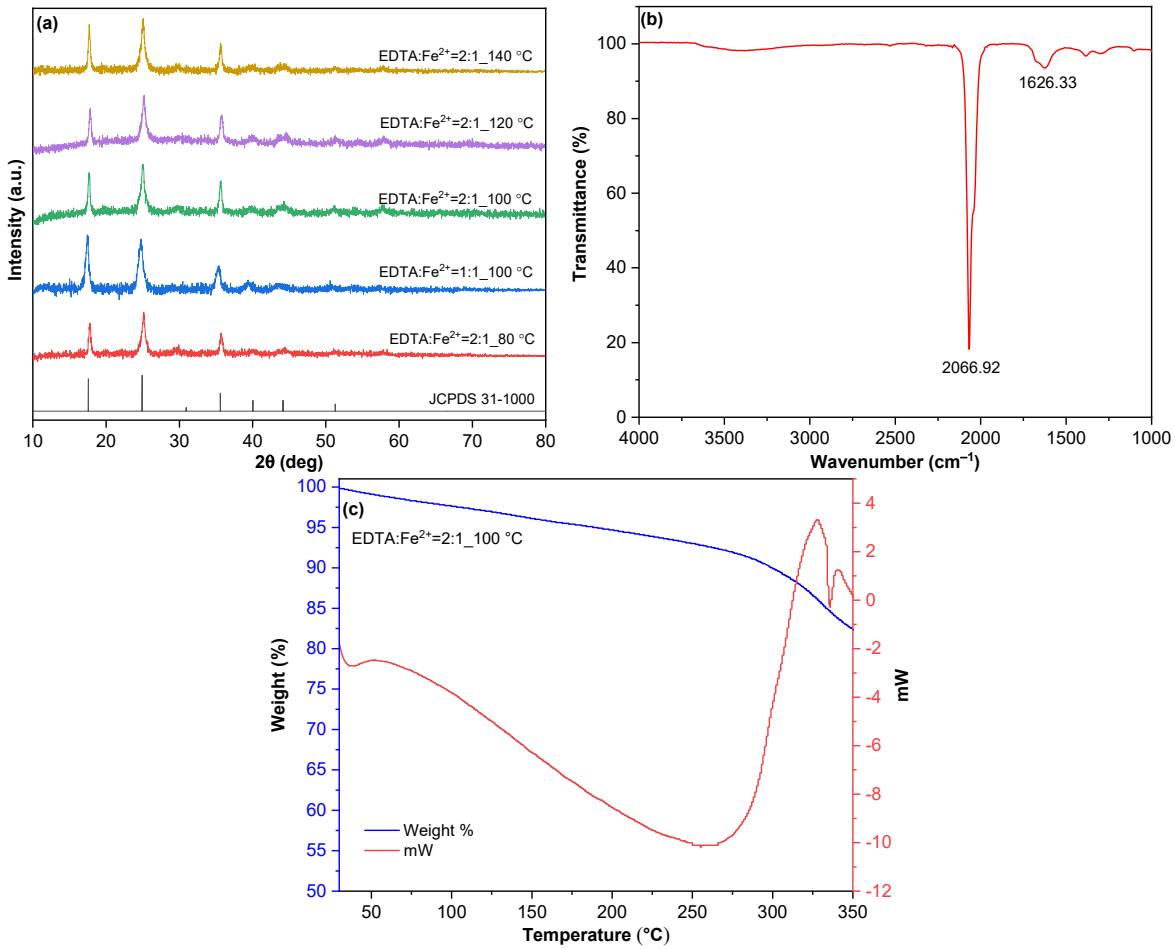

Fig 1. (a) XRD patterns of different KFHCF samples, (b) FTIR spectrum, and (c) TGA result of KFHCF (2:1_100 °C) sample

cubic structure (FCC) with space group Fm-3m, confirming the formation of Prussian white KFHCF. Additionally, the high intensity of these diffraction peaks suggests that the material is highly crystalline, with a well-defined crystal structure. The crystal size of the KFHCF samples synthesized at different chelating ratios and drying temperatures was calculated using Scherrer's Eq. (1) and is presented in Table 1 [19-20];

$$D = \frac{k\lambda}{\beta \cos\theta} \quad (1)$$

where k is the Scherrer coefficient equal to 0.94; β is the full width at half maximum (FWHM); λ is the X-ray wavelength; θ is the Bragg diffraction angle of the XRD peak.

The observed difference in crystal size between the two molar ratios suggests that the ratio of the chelating agent significantly influences the crystallization process and resulting particle size. Specifically, at a lower 1:1 molar ratio, the fast precipitation reaction kinetics appear to alter the crystallization process, reducing crystal size. This observation underscores the importance of the chelating agent ratio as a critical parameter in controlling the nucleation and growth of particles during the synthesis of KFHCF.

FTIR spectroscopy was applied to analyze the typical and distinctive functional groups of the material, particularly focusing on water molecules and cyanide complexes. The analysis was conducted on a sample synthesized with an EDTA:Fe^{2+} molar ratio of 2:1 and dried at 100 °C, with results shown in Fig. 1(b). In the FTIR curve of KFHCF sample, distinct characteristic signals corresponding to water molecules and cyanide complex groups are observed. The presence of water molecules is confirmed by a peak at 1626 cm^{-1}, corresponding to the bending modes of the H–O–H bond in H_2O, indicating that the hydrating process of water molecules is the reason for the H_2O presence in the interstitial sites of the material. Interestingly, the absence of a signal in the 3200 and 3300 cm^{-1} range, typically associated with the O–H stretching mode of H_2O, suggests a low residual water content in this sample. A strong, singular peak observed around 2067 cm^{-1}, is attributed to the stretching vibration of the C≡N triple bond of the cyanide-coordinated Fe^{2+}. This peak aligns with data from related cyanide complexes [21]. Notably, there are no signals indicating the presence of the centers [22], confirming that the potassium iron hexacyanoferrate sample contains only divalent iron. The KFHCF sample was prepared with a chelating ratio of 2:1 between EDTA and Fe^{2+}, then dried in a vacuum environment at 100 °C for 10 h. TGA analysis was applied to estimate the water content and the thermal stability of this sample. The analysis was performed in a nitrogen-controlled atmosphere, heating the sample from ambient temperature to 350 °C with a rate of 5 °C min^{-1}. As shown in Fig. 1(c), the TGA curve reveals two distinct weight loss stages as the temperature increases from 25 to 350 °C. The first stage, occurring around 150 °C, shows a 4% weight loss, which can be attributed to the evaporation of coordinated water molecules, consistent with the FTIR result for this sample. The second stage, occurring between 250 to 350 °C, indicates the decomposition of the material, accompanied by the release of toxic HCN gas. Based on the TGA results, the chemical formula for a nearly ideal sample at 150 °C is given as $K_2Fe[Fe(CN)_6]\cdot 0.04H_2O$, indicating the presence of a small number of water molecules.

To analyze the morphology of the materials, SEM was performed on the sample synthesized with the different molar ratio of EDTA:Fe^{2+} = 1:1 or 2:1 and dried

Table 1. Crystallite size of KFHCF samples

Sample	EDTA:Fe^{2+}	Drying temperature (°C)	β (FWHM)	2θ (°)	D (nm)
KFHCF	2:1	80	0.718	25.1392	11.34
		100	0.717	25.0310	11.36
		120	0.807	25.1803	10.08
		140	0.706	25.0669	11.52
	1:1	100	0.846	24.7699	9.61

at 80, 100, 120, and 140 °C, as shown in Fig. 2. Overall, all the samples exhibit well-packed cubic morphology. However, some non-uniform and agglomerated nanoparticles are also present. The effect of the chelating ratio between EDTA and Fe^{2+} on the material properties is particularly noteworthy. Samples prepared with a 2:1 chelating ratio show an average edge length of approximately 50 nm, whereas those with a 1:1 ratio display a smaller particle size of around 30 nm. This suggests that a higher chelating ratio contributes to higher crystallinity, improved particle size, and better morphology. Large particle sizes are often preferred for cathode materials in batteries, as they can provide better electrochemical performance and stability [21].

As illustrated in Fig. 3(a), all the KFHCF samples exhibit the same trendline at a scan rate of 10 mV s^{-1}. The CV curves generally display two pairs of well-separated redox peaks at 0.3/0.1 V and 0.9/0.8 V, which correspond to the Fe^{2+}/Fe^{3+} couples. The low-potential peaks originate from the redox process on the Fe^{2+} site with a high-spin configuration coordinating with nitrogen, while the high-potential peaks are derived from the redox process on the Fe^{2+} site with a low-spin configuration that coordinates with carbon [23]. These two redox processes can be described by Eq. (2). Interestingly, at a 1:1 molar ratio of EDTA:Fe^{2+}, the sample dried at 100 °C displayed the highest redox peaks with the current density of 4.5 mA cm^{-2} of the high-spin Fe^{2+} site and 4 mA cm^{-2} for the low-spin Fe^{2+} site accompanied by a larger peak area compared to the sample dried at 80 and 120 °C.

$$K_2Fe^{II}\left[Fe^{II}(CN)_6\right] \leftrightarrow KFe^{III}\left[Fe^{II}(CN)_6\right] + K^+ + e^- \leftrightarrow Fe^{III}\left[Fe^{III}(CN)_6\right] + K^+ + e^- \quad (2)$$

In Fig. 3(b), the KFHCF samples were prepared with a molar ratio of chelating agent EDTA:Fe^{2+} = 2:1 and dried at various temperatures (80, 100, 120, and 140 °C) in a vacuum environment for 10 h. The CV curves also demonstrate two well-separated pairs of redox peaks, occurring at approximately 0.3/0.1 V and 0.9/0.8 V, which correlate with the Fe^{2+}/Fe^{3+} couples, as shown in Fig. 3(a). Specifically, the redox peak of samples dried at 100 and 120 °C exhibits higher current densities, around 4 mA cm^{-2} for both the high-spin and low-spin Fe^{2+} sites, with a larger area compared to those dried at 80 °C. However, when the drying temperature is increased to 140 °C, the redox peak current densities reduce by nearly half. The provided CV curves indicate that the drying temperature significantly influences the electrochemical behavior of the material during its synthesis. Notably, the sample dried at 100 °C exhibits superior electrochemical performance compared to samples dried at lower or higher temperatures. To compare the

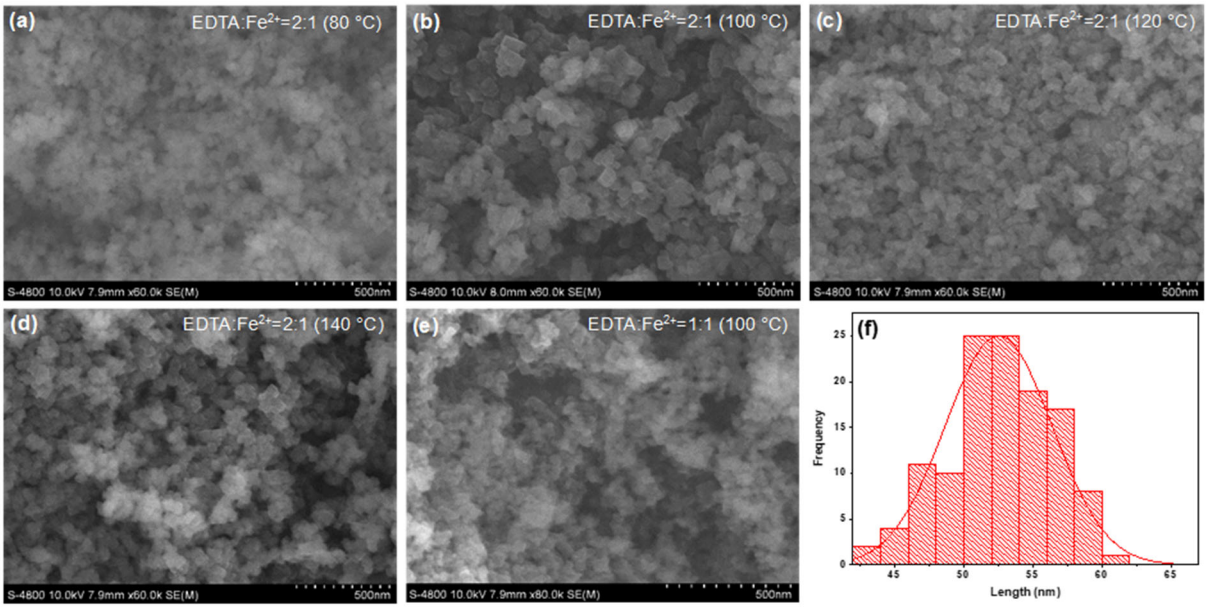

Fig 2. (a–e) SEM images of KFHCF samples and (f) distribution column of average edge length

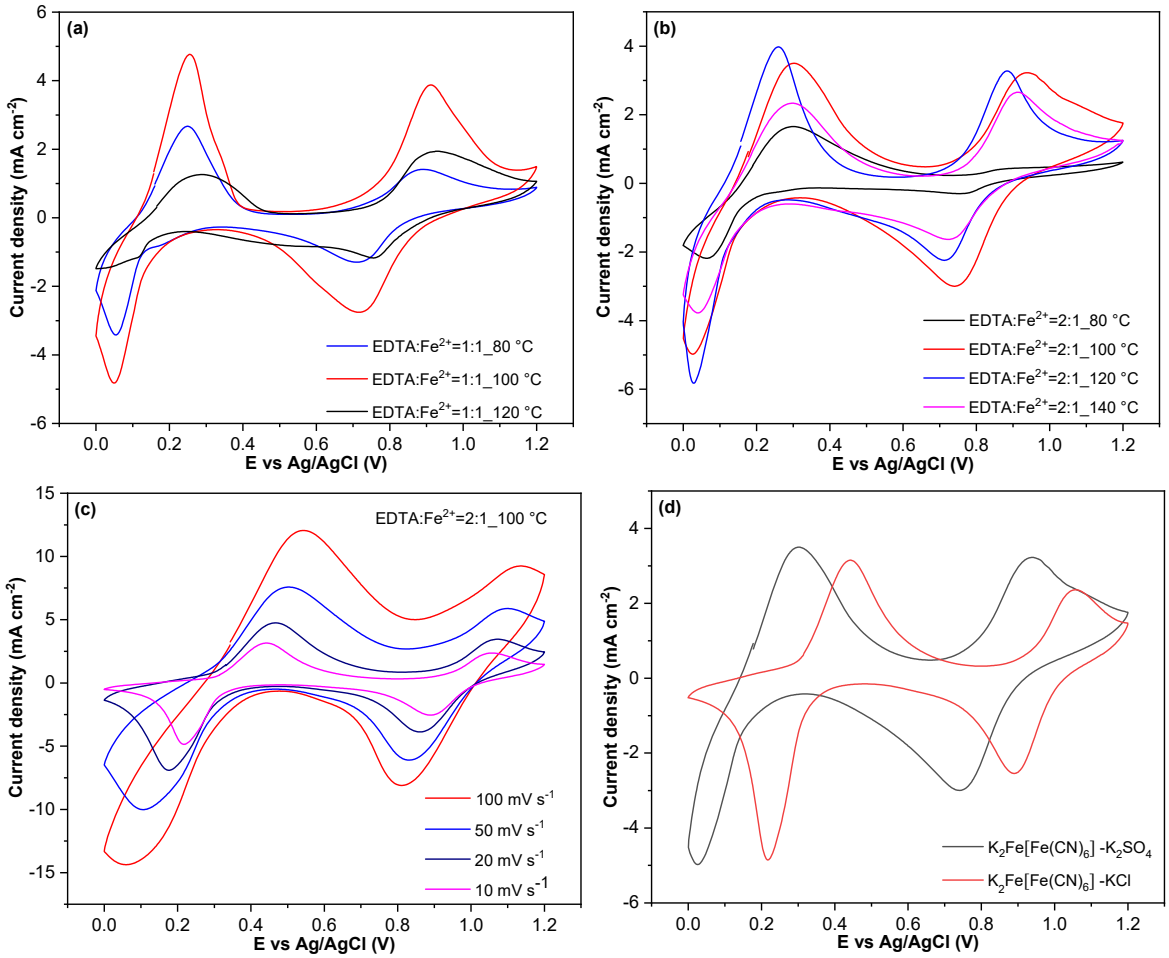

Fig 3. CV curves of KFHCF samples at (a) 1:1 and (b) 2:1 molar ratio of EDTA:Fe^{2+} in K_2SO_4 electrolyte at a scan rate of 10 mV s^{-1}; (c) KFHCF (EDTA:Fe^{2+} = 2:1_100 °C) samples in KCl electrolyte at scan rates of 100, 50, 20, and 10 mV s^{-1}; (d) comparison between K_2SO_4 and KCl electrolytes at a scan rate of 10 mV s^{-1}

electrochemical activity of all the synthesized samples in terms of battery performance, the capacitance and charge stored calculations were conducted using Eq. (3) and (4). The results, summarized in Table 2 provide a detailed comparison of the capacitance and charge performance of all samples [24-25];

$$C = \frac{\int I.dV}{m.s.U} \quad (3)$$

$$Q = C.U \quad (4)$$

where, $\int I.dV$ is the scanning area (mAV), m is the material mass (g), s is the scanning rate (mV s^{-1}), U is potential (V), Q is capacity (mAh g^{-1}), and C is the capacitance (F g^{-1}).

As shown in Table 2, the capacity values of KFHCF samples were calculated by Eq. (2) and (3) from CV results with a molar ratio of EDTA:Fe^{2+} (1:1) with a molar ratio of EDTA:Fe^{2+} (2:1) at 80, 120, 100, and 120 °C. From Table 2, the materials synthesized at 100 °C exhibit high stored charge values of 71.35 and 74.13 mAh g^{-1}, respectively. However, the capacitance and stored charge values decrease for both molar ratios at a higher or lower drying temperature. From these results, it is clear that this material exhibits a high theoretical capacity and performance, particularly at the 2:1 molar ratio of chelating agent to free Fe^{2+} ions and high drying temperature, specifically at 100 °C. Based on the discussed data, the sample prepared with a 2:1 molar ratio of EDTA to Fe^{2+} and dried at 100 °C in a vacuum environment is the most appropriate for achieving optimal electrochemical performance.

As observed in Fig. 3(c), the CV curves at different

Table 2. The electrochemical activity of KFHCF samples in K_2SO_4 electrolyte at a scan rate 10 mV s^{-1}

Temperature (°C)	EDTA:Fe^{2+} (molar ratio)	Capacity (mAh g^{-1})
80	1:1	37.22
100		71.35
120		35.07
80	2:1	21.49
100		74.13
120		62.85
140		51.11

scan rates of the KFHCF sample display a consistent trendline with two pairs of well-separated redox peaks corresponding with the Fe^{2+}/Fe^{3+} couples. Furthermore, the current densities increase higher than in K_2SO_4 aqueous electrolyte. Interestingly, in both electrolytes, two pairs of redox peaks occur. However, the positions of the peaks are different because the operating voltage of the KFHCF sample in the KCl electrolyte is higher than that in the K_2SO_4 electrolyte. In the KCl electrolyte, the redox peaks are shifted to 0.4/0.2 V and 1.1/0.9 V for both Fe^{2+} coordination sites, as shown in Fig. 3(d). The difference in operating voltage between the two electrolytes indicates the influence of the electrolyte composition on the redox behavior of the KFHCF material. Specifically, SO_4^{2-} is more complex and bulkier than Cl^-, which might inhibit K^+ transport during the electrochemical process, resulting in lower operating voltage. Therefore, the presence of specific ions in the electrolyte can affect the thermodynamics and kinetics of the redox reaction.

The discharge capacity of the KFHCF sample was measured in an aqueous electrolyte (K_2SO_4), with a potential range from 0–1.2 V, while the current densities varied from 500–750–1000 mA g^{-1}. During the discharge process, as shown in Fig. 4(a), there are two distinct discharge plateaus at 0.8 and 0.2 V, respectively, consistent with the CV results and corresponding to the potassium-ion intercalation associated with two coordination sites. Specifically, the plateau at 0.8 V represents the reduction process on the Fe^{2+} site with a low-spin configuration that coordinates with carbon, while the plateau at 0.2 V is derived from the reduction process on the Fe^{2+} site with a high-spin configuration coordinating with nitrogen.

At a current density of 500 mA g^{-1}, the electrode initially exhibited a discharge capacity of 113.97 mAh g^{-1}, which then decreased to 103.01 mAh g^{-1} at 750 mA g^{-1}, and 94.51 mAh g^{-1} at 1000 mA g^{-1}. These findings align with previous studies

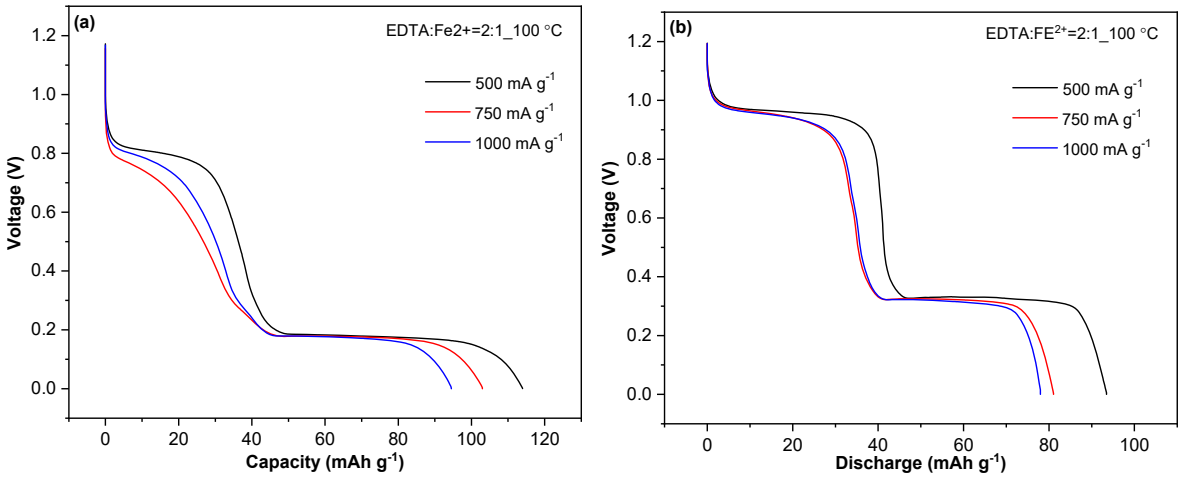

Fig 4. The discharge voltage profiles of KFHCF samples with (a) K_2SO_4 and (b) KCl electrolytes at current densities at 500, 750, and 1000 mA g^{-1}

by Su et al. [18] regarding the discharge capacity of KFHCF material, indicating the reproducibility and consistency of the observed discharge behavior. Moreover, the capacity of KFHCF material at 750 mA g^{-1} (103.01 mAh g^{-1}) is higher than Xu's result (96.1 mAh g^{-1}) for sodium manganese iron-based Prussian material [12].

As shown in Fig. 4(b), the KFHCF material exhibited two distinct voltage plateaus centered at 0.9 and 0.3 V during the discharge process in the KCl aqueous electrolyte, which is in agreement with the CV results, corresponding to the potassium-ion intercalation associated with two coordination sites. The voltage plateau at 0.95 V is attributed to the reduction process on the Fe^{2+} site with a low-spin configuration that coordinates with carbon, while the plateau at 0.3 V originates from the reduction process on the Fe^{2+} site with a high-spin configuration coordinating with nitrogen. The operating voltage of KFHCF material is higher and the discharge curve presented for two reduction processes of both Fe^{2+} sites is quite uniform and consistent.

Although the KCl aqueous electrolyte provides a convenient environment for ion transportation, the capacitance of the KFHCF material during the potassium-ion intercalation process is not as high as observed in the K_2SO_4 aqueous electrolyte. Overall, the different electrolyte compositions may influence ion diffusion, redox reactions, and overall charge storage capabilities. At 500 mA g^{-1}, an initial discharge capacity of 93.45 mAh g^{-1} is achieved, which decreases to 81.03 mAh g^{-1} at 750 mA g^{-1}, and further reduces to 78 mAh g^{-1} at 1000 mA g^{-1}.

The cycling performance of the KFHCF sample in a KCl aqueous electrolyte is illustrated in Fig. 5. After 20 cycles, a reversible discharge capacity of 79.4 mAh g^{-1} with a capacity retention of 80% was achieved at 1000 mA g^{-1}, suggesting that the electrode can sustain its performance over a certain number of cycles. Notably, during the first five cycles, the electrode still delivered a reversible capacity of ~95 mAh g^{-1}, with two uniform reduction plateaus on both Fe^{2+} sites, indicating the reversible capabilities of the material.

■ CONCLUSION

The KFHCF sample prepared at a 2:1 molar ratio between EDTA-2K and $FeCl_2$; and dried at 100 °C in 10 h under a vacuum environment exhibits a higher current density of 7.1 mA cm^{-2} for both redox peaks of the Fe^{2+} site, compared to other samples. The XRD pattern and SEM image reveal high crystallization within the structure and well-packed cubic particles with a size of approximately 50 nm, while the TGA result confirms the chemical formula of this sample as $K_2Fe[Fe(CN)_6]\cdot 0.04H_2O$. In a K_2SO_4 aqueous electrolyte, this material exhibits two redox peaks at 0.3/0.1 and 0.9/0.8 V with current densities of 4 mA cm^{-2}, delivering

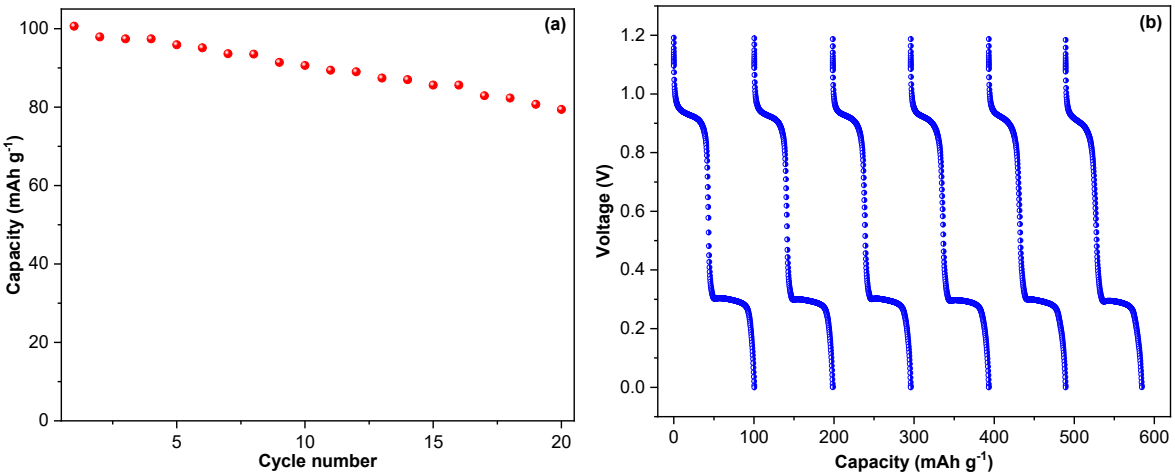

Fig 5. (a) Cycling performance (20th cycles) and (b) discharge capacities versus cycle number (last six cycles) of KFHCF sample in KCl aqueous electrolyte at 1000 mA g^{-1}

a discharge capacity of 113.97 mAh g^{-1}. In contrast, when tested in the KCl aqueous electrolyte, the redox peaks shift to 0.4/0.2 and 1.1/0.9 V, with current densities increasing to approximately 5 mA cm^{-2} and delivering a discharge capacity of 93.45 mAh g^{-1}. Moreover, the capacity retention of KFHCF was obtained at 80% after 20 discharge cycles in KCl aqueous electrolytes at 1000 mA g^{-1}. This comparison suggests that the KCl electrolyte can improve the ion diffusion and thus enhance the operating voltage of the material.

■ ACKNOWLEDGMENTS

We acknowledge HCMUT and VNU-HCM for supporting this study.

■ CONFLICT OF INTEREST

The authors have no conflict of interest to declare.

■ AUTHOR CONTRIBUTIONS

Minh Vien Le: Conceptualization, Formal analysis, Investigation, Methodology, Visualization, Writing-Review & Editing. Nguyen Tan Dat: Visualization, Writing-Review & Editing. Ly Dat: Formal analysis, Investigation, Methodology, Do Ngoc Nhu Quynh: Formal analysis, Methodology, Van Hoang Luan: Conceptualization, Writing-Original Draft, Writing & Editing, Methodology, Supervision.

■ REFERENCES

[1] Sasi Bhushan, M.A., Sudhakaran, M., Dasarathan, S., and Mariappane, E., 2025, Integration of a heterogeneous battery energy storage system into the Puducherry smart grid with time-varying loads, *Energies*, 18 (2), 428.

[2] Wan, J., Wang, R., Liu, Z., Zhang, L., Liang, F., Zhou, T., Zhang, S., Zhang, L., Lu, Q., Zhang, C., and Guo, Z., 2023, A double-functional additive containing nucleophilic groups for high-performance Zn-Ion batteries, *ACS Nano*, 17 (2), 1610–1621.

[3] Vanderbruggen, A., Sygusch, J., Rudolph, M., and Serna-Guerrero, R., 2021, A contribution to understanding the flotation behavior of lithium metal oxides and spheroidized graphite for lithium-ion battery recycling, *Colloids Surf., A*, 626, 127111.

[4] Sanguesa, J.A., Torres-Sanz, V., Garrido, P., Martinez, F.J., Marquez-Barja, and J.M., 2021, A review on electric vehicles: Technologies and challenges, *Smart Cities*, 4 (1), 372–404.

[5] Blomgren, G.E., 2017, The development and future of lithium ion batteries, *J. Electrochem. Soc.*, 164, A5019.

[6] Nitta, N., Wu, F., Lee, J.T., and Yushin, G., 2015, Li-ion battery materials: Present and future, *Mater. Today*, 18 (5), 252–264.

[7] Liu, Y., and Holze, R., 2022, Metal-ion batteries, *Encyclopedia*, 2 (3), 1611–1623.

[8] Masias, A., 2018, "Lithium-Ion Battery Design for Transportation" in *Behavior of Lithium-Ion Batteries in Electric Vehicles: Battery Health, Performance, Safety, and Cost*, Eds. Pistoia, G., and Liaw, B., Springer International Publishing, Cham, Switzerland, 1–34.

[9] Phogat, P., Dey, S., and Wan, M., 2025, Comprehensive review of sodium-ion batteries: Principles, materials, performance, challenges, and future perspectives, *Mater. Sci. Eng., B*, 312, 117870.

[10] Wu, Z., Zou, J., Zhang, Y., Lin, X., Fry, D., Wang, L., and Liu, J., 2022, Lignin-derived hard carbon anode for potassium-ion batteries: Interplay among lignin molecular weight, material structures, and storage mechanisms, *Chem. Eng. J.*, 427, 131547.

[11] Ji, B., Yao, W., Zheng, Y., Kidkhunthod, P., Zhou, X., Tunmee, S., Sattayaporn, S., Cheng, H.M., He, H., and Tang, Y., 2020, A fluoroxalate cathode material for potassium-ion batteries with ultra-long cyclability, *Nat. Commun.*, 11 (1), 1225.

[12] Xu, L., Liu, Y., Chen, M., Wu, W., Qiu, S., Wu, H., Zheng, M., Zhang, X., and Wu, X., 2025, Suppressing vacancies and crystal water of sodium manganese iron-based Prussian blue analogue by potassium doping for advanced sodium-ion batteries, *Chem. Eng. Sci.*, 302, 120848.

[13] Kubota, K., Dahbi, M., Hosaka, T., Kumakura, S., and Komaba, S., 2018, Towards K-ion and Na-ion batteries as "beyond Li-ion", *Chem. Rec.*, 18 (4), 459–479.

[14] Komaba, S., Hasegawa, T., Dahbi, M., and Kubota, K., 2015, Potassium intercalation into graphite to

realize high-voltage/high-power potassium-ion batteries and potassium-ion capacitors, *Electrochem. Commun.*, 60, 172–175.

[15] Saju, S.K., Chattopadhyay, S., Xu, J., Alhashim, S., Pramanik, A., and Ajayan, P.M., 2024, Hard carbon anode for lithium-, sodium-, and potassium-ion batteries: Advancement and future perspective, *Cell Rep. Phys. Sci.*, 5 (3), 101851.

[16] Mandai, T., Dokko, K., and Watanabe, M., 2019, Solvate ionic liquids for Li, Na, K, and Mg batteries, *Chem. Rec.*, 19 (4), 708–722.

[17] Bie, X., Kubota, K., Hosaka, T., Chihara, K., and Komaba, S., 2017, A novel K-ion battery: Hexacyanoferrate(II)/graphite cell, *J. Mater. Chem. A*, 5 (9), 4325–4330.

[18] Su, D., McDonagh, A., Qiao, S.Z., and Wang, G., 2017, High-capacity aqueous potassium-ion batteries for large-scale energy storage, *Adv. Mater.*, 29 (1), 1604007.

[19] Bommier, C., Mitlin, D., and Ji, X., 2018, Internal structure – Na storage mechanisms – Electrochemical performance relations in carbons, *Prog. Mater. Sci.*, 97, 170–203.

[20] Batool, M., Haider, M.N., and Javed, T., 2022, Applications of spectroscopic techniques for characterization of polymer nanocomposite: A review, *J. Inorg. Organomet. Polym. Mater.*, 32 (12), 4478–503.

[21] Ghosh, S.N., 1974, Infrared spectra of the Prussian blue analogs, *J. Inorg. Nucl. Chem.*, 36 (11), 2465–2466.

[22] Hosaka, T., Kubota, K., Hameed, A.S., and Komaba, S., 2020, Research development on K-ion batteries, *Chem. Rev.*, 120 (14), 6358–6466.

[23] Liu, S., Meyer, L.C., Medenbach, L., and Balducci, A., 2022, Glyoxal-based electrolytes for potassium-ion batteries, *Energy Storage Mater.*, 47, 534–541.

[24] Mirzaee, M., and Pour, G.B., 2018, Design and fabrication of ultracapacitor based on paper substrate and $BaTiO_3$/PEDOT: PSS separator film, *Recent Pat. Nanotechnol.*, 12, 192–199.

[25] Kurzweil, P., Frenzel, B., and Scheuerpflug, W., 2022, A novel evaluation criterion for the rapid estimation of the overcharge and deep discharge of lithium-ion batteries using differential capacity, *Batteries*, 8 (8), 86.